IVYSPRING INTERNATIONAL PUBLISHER

Theranostics

2018; 8(2): 314-327. doi: 10.7150/thno.19010

Research Paper

Tumour Vascular Shutdown and Cell Death Following Ultrasound-Microbubble Enhanced Radiation Therapy

Ahmed El Kaffas[2, 3, 4], Mehrdad J. Gangeh[2, 3], Golnaz Farhat[1, 2], William Tyler Tran[2], Amr Hashim[1], Anoja Giles[1], Gregory J. Czarnota[1, 2, 3]✉

1. Physical Sciences, Sunnybrook Research Institute, Toronto, ON, M4N 3M5 Canada;
2. Department of Radiation Oncology, Sunnybrook Health Sciences Centre, Toronto, ON, M4N 3M5 Canada;
3. Departments of Medical Biophysics, and Radiation Oncology, University of Toronto, Toronto, ON, M4N 3M5 Canada;
4. Department of Radiology, School of Medicine, Stanford University, 1201 Welch Rd., Palo Alto, CA, 94304.

✉ Corresponding author: Gregory J. Czarnota gregory.czarnota@sunnybrook.ca 2075 Bayview Avenue, Room T2-177, Toronto, ON M4N 3M5 CANADA Tel. 416-480-6100 x 6128, Fax. 416-480-6002

Received: 2017.01.01; Accepted: 2017.08.11; Published: 2018.01.01

Abstract

High-dose radiotherapy effects are regulated by acute tumour endothelial cell death followed by rapid tumour cell death instead of canonical DNA break damage. Pre-treatment with ultrasound–stimulated microbubbles (USMB) has enabled higher-dose radiation effects with conventional radiation doses. This study aimed to confirm acute and longitudinal relationships between vascular shutdown and tumour cell death following radiation and USMB in a wild type murine fibrosarcoma model using *in vivo* imaging.

Methods: Tumour xenografts were treated with single radiation doses of 2 or 8 Gy alone, or in combination with low-/high-concentration USMB. Vascular changes and tumour cell death were evaluated at 3, 24 and 72 h following therapy, using high-frequency 3D power Doppler and quantitative ultrasound spectroscopy (QUS) methods, respectively. Staining using *in situ* end labelling (ISEL) and cluster of differentiation 31 (CD31) of tumour sections were used to assess cell death and vascular distributions, respectively, as gold standard histological methods.

Results: Results indicated a decrease in the power Doppler signal of up to 50%, and an increase of more than 5 dBr in cell-death linked QUS parameters at 24 h for tumours treated with combined USMB and radiotherapy. Power Doppler and quantitative ultrasound results were significantly correlated with CD31 and ISEL staining results ($p < 0.05$), respectively. Moreover, a relationship was found between ultrasound power Doppler and QUS results, as well as between micro-vascular densities (CD31) and the percentage of cell death (ISEL) (R^2 0.5-0.9).

Conclusions: This study demonstrated, for the first time, the link between acute vascular shutdown and acute tumour cell death using *in vivo* longitudinal imaging, contributing to the development of theoretical models that incorporate vascular effects in radiation therapy. Overall, this study paves the way for theranostic use of ultrasound in radiation oncology as a diagnostic modality to characterize vascular and tumour response effects simultaneously, as well as a therapeutic modality to complement radiation therapy.

Key words: ultrasound therapy and imaging, ultrasound treatment monitoring, power Doppler, quantitative ultrasound spectroscopy, ultrasound-stimulated microbubbles, radiation therapy, vascular targeting.

Introduction

Radiotherapy is a common therapeutic modality for cancer treatment. It is canonical in radiobiology that radiotherapy acts by direct or indirect damage to the DNA of cancer cells, which in-turn prevents tumour cell proliferation, leading to cell death (1,2). Recent studies in pre-clinical murine models suggest that tumour endothelial cells preferentially and acutely respond to single high doses (> 8-22 Gy) of radiation, and that inhibiting radiation-based tumour vascular responses minimizes the overall tumour response to treatment (3–7). These studies suggest that tumour vasculature is an important regulator of tumour response to radiation (6,8). More specifically, these posit that acute vascular shutdowns result in

rapid tumour cell death that directly contributes to the observed enhancement in tumour radiation-response (Figure 1A). Such observed vascular responses have been linked to ceramide-dependant apoptosis signalling mechanisms that are triggered by the upregulation of acid-sphingomyelinase (ASMase) in the membrane of cells (5, 9, 10). Studies have suggested the use of conventional vascular targeting agents, such as anti-angiogenics, to radiosensitize tumour endothelial cells to lower (< 6 Gy) radiation doses (6, 7, 11–13). More recently, ultrasound-stimulated microbubbles (USMB) have been demonstrated as novel mechanobiology-based vascular targeting agents with the ability to increase endothelial cell radiosensitivity (12, 14–16).

Microbubbles are micron-sized (2-12 μm) spheres, typically filled with gas or air, and enclosed within a biocompatible protein or lipid shell material. These are commonly used as ultrasound contrast agents, yielding tissue perfusion information (17). A number of new therapeutic applications have been proposed that leverage the biomechanical effects of these mechano-acoustic agents (18). Of particular interest is the use of microbubbles as endothelial radiosensitizers (12, 16, 19). Localized stimulation of microbubbles with ultrasound mechanically perturbs endothelial cell membranes, thus resulting in the activation of a ceramide-based biomechanical pathway that enhances endothelial cell radiosensitivity, reminiscent of that described above. Treatment with radiation subsequently results in acute vascular disruption (shutdown) and an overall improved tumour response to both low (2-4 Gy) and high (> 8 Gy) doses of radiation. While both high-dose radiation and USMB-based effects have been evaluated using immunohistological methods, no longitudinal *in vivo* treatment monitoring has been used to confirm a direct relationship between vascular shutdown and tumour cell death.

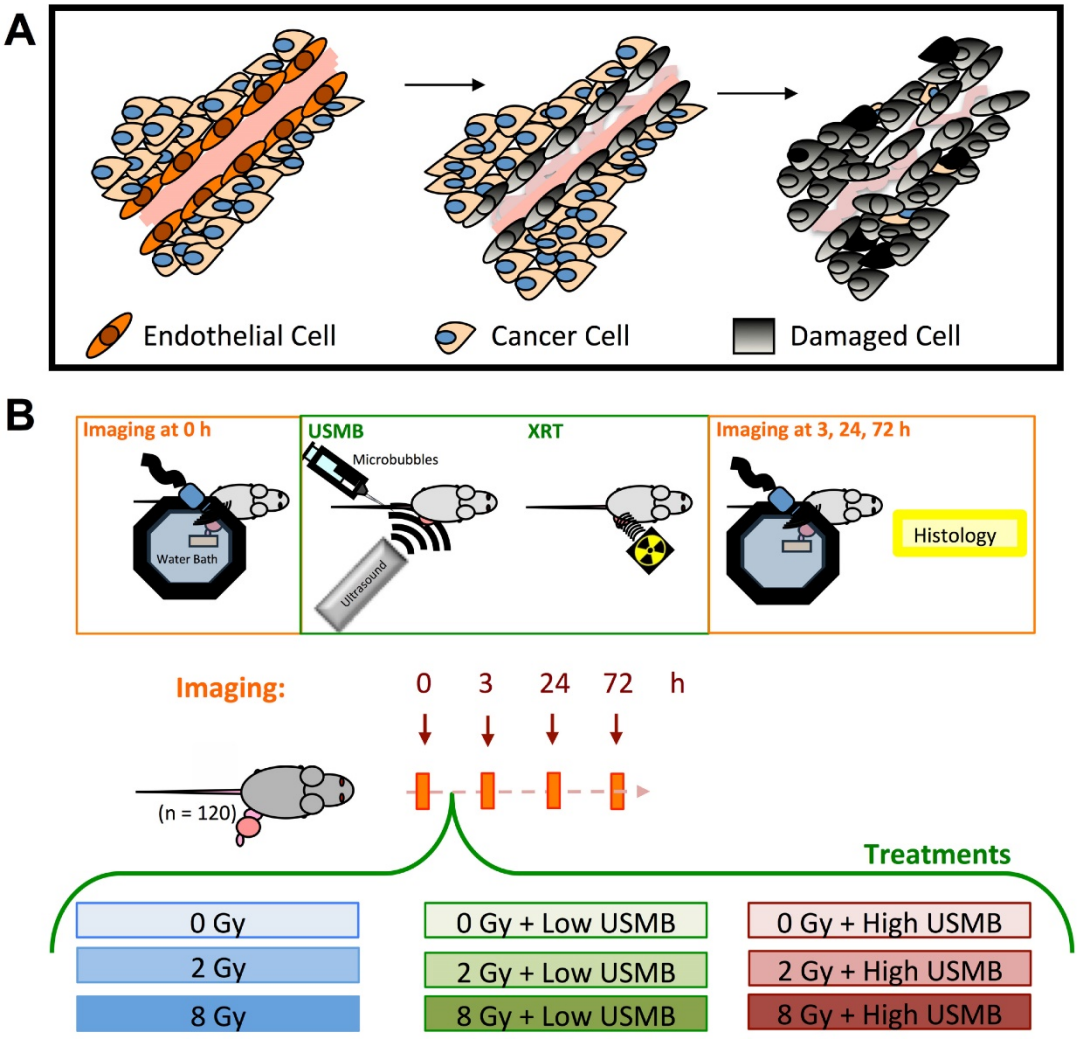

Figure 1. (A) Schematic of experimental workflow, imaging time points and treatment conditions. (B) Illustration of events causing tumour cell death where endothelial cells are primary responders/target, followed by tumour cell death.

In this work, we have investigated the relationship between acute vascular disruption and tumour cell death at different times following microbubble-radiation-based vascular targeting therapy. Animal tumours were treated with a low (2 Gy) or a high (8 Gy) dose of radiation alone, or in combination with ultrasound-stimulated microbubbles (USMB) (Figure 1B). Treatment responses were assessed at 3, 24, or 72 h after the start of treatment. Volumetric high frequency ultrasound was used to investigate the effects of treatment on tumour vasculature and tumour cell death. More specifically, volumetric power Doppler ultrasound was utilized to monitor tumour vascular responses in longitudinal studies (20–22). Furthermore, power Doppler, quantitative ultrasound spectroscopy (QUS) methods were used to assess acute tumour responses to prescribed therapies (23–27). In addition to ultrasound, we collected tumours post-mortem to assess cell death and micro-vascular densities using standard immunohistological methods (CD31 and ISEL).

Methods and Materials

Animal Tumour Model

All animal experiments presented in this work were conducted in compliance with internationally recognized guidelines specified in protocols approved by the Sunnybrook Research Institute Institutional Animal Care and Use Committee. MCA-129 fibrosarcoma cells were cultured in DMEM (Wisent Inc., Montreal, QC), supplemented with 10% Characterized Fetal Bovine Serum (Hyclone, Logan, UT) and 1% Penicillin Streptomycin (Gibco, Grand Island, NY), and incubated at 37°C in a humidified incubator, maintained at 5% CO_2. Cells were trypsinized (Gibco, Grand Island, NY), pooled and counted. A total of $1x10^6$ cells suspended in 50 µl of phosphate-buffered saline (PBS) were injected into the right hind leg of wild type C57BL/6 mice. This type of mouse was shown to be compatible with the cell lines used (5,9). Tumours were grown for approximately 10 days, reaching an average diameter of 1.0 cm at the time of experiments. A total of 108 animals were used for this study.

Treatment

Mice were anesthetised via subcutaneous injection prior to treatment using a mixture of ketamine (100 mg/kg), xylazine (5 mg/kg) and acepromazine (1 mg/kg). Animals were kept warm using heat lamps and/or heat pads in order to maintain their regular body temperature and normal blood flow during treatment and imaging. Definity® microbubbles were used for USMB (Lantheus Medical Imaging Inc., N. Billerica, MA). Definity® bubbles were activated as instructed by the manufacturer using a Vialmix® (Lantheus Medical Imaging Inc., N. Billerica, MA) for 45 s. According to the manufacturer, this resulted in the formation of microbubbles with a mean diameter ranging from 1.1 µm to 3.3 µm and a maximum diameter of 20 µm. For USMB therapy, the treatment set-up was based on previously published studies, which includes optimization of ultrasound parameters and timing (11,12,15,28–30). During USMB therapy, animals were mounted on an acrylic jig, which was then submerged in a 37°C water bath within the focal range of a 500 kHz linear transducer (IL0509HP; ValpeyFisher Inc.). This was attached to a micropositioning system and excited with a sinusoidal wave generated by a waveform generator (AWG520; Tektronix), a pulse-receive power amplifier (RPR4000; Ritec Inc.), and a digital-acquisition system (Acquiris CC103, Agiulent Technologies NY). Tumours were exposed over 50 ms to a 16-cycle tone burst at 500 kHz and 3 kHz pulse repetition frequencies with a 10% duty cycle during the 50 ms window. The treatment duration was 5 min, amounting to a 750 ms exposure over 5 min for all mouse treatments, with an average duty cycle of 0.25%. Specifically, at 500 kHz the pulse bandwidth of the 16-cycle tone burst was 31.3 KHz. The pulse repetition period (3-KHz pulse repetition frequency) was 0.333 ms, which, over 50 ms, corresponded to 150 periods of 16-cycle tone burst or 4.8 ms (rounded to 5 ms) (12,15,28,31). This 5 ms time occurred every 2 s to permit blood vessels to refill with bubbles during a treatment time of 5 min (300 s), or 150 times, for a total time of 750 ms. The ultrasound peak negative pressure was 570 kPa measured with a calibrated hydrophone (Sonora Medical Systems Inc, Longmont, CO) (15,31). The -6 dB beamwidth was 31 mm and the -3 dB beamwidth was 18 mm. The head of the animal remained dry, while only the hind legs were submerged, carefully placing the tumour volume at the natural peak focus of the ultrasound transducer, and subsequently exposing only the tumour volume to the ultrasound field. Microbubbles were then diluted in saline (25 µL of microbubbles in 75 µL of saline for 1% and 70 µL of microbubbles in 30 µL of saline for 3%) and intravenously injected into the tail vein via catheter during insonification. A total of 100 µL of the microbubble solution at low (1% v/v) or high (3% v/v) concentration according to total animal blood volume estimated by its weight was injected at a constant rate, followed by 150 µL of saline with 0.2% heparin. Microbubbles were stimulated within the tumour volume as above. Tumours were subjected to ultrasound treatment for a total of 5 min, and immediately irradiated afterwards. More details

about the treatment set-up are presented in Supplementary Figures S1 and S2.

Radiation therapy was administered with a Faxitron cabinet irradiator (Faxitron Bioptics, Lincolnshire, IL) using X-rays at an energy of 160 kVp, a source to surface distance (SSD) of 35 cm, and a dose rate of 200 cGy/min. Radiation doses used were 2 Gy and 8 Gy in single doses, administered alone, or immediately after USMB. Animals were covered with a 3 mm thick lead shielding, exposing only the tumour volume to radiation. A total of 4-5 animals were used in each of the 27 therapeutic conditions (0 Gy, 2 Gy, 8 Gy; No USMB, Low USMB, High USMB; 3 h, 24 h, 72 h).

In Vivo Imaging

High-frequency volumetric power Doppler ultrasound was used to assess overall tumour responses to administered treatments. The modality allowed imaging whole 3D volumes as opposed to single 2D planes, as is often the case in other vascular imaging methods and immunohistological assays (7). At high frequencies, power Doppler ultrasound can detect flow signals of 1-2 mm/s in vessels that are greater than 30 µm in diameter and are up to 25 mm below the skin surface. Data was acquired using a VEVO770 high-frequency ultrasound-imaging device (VisualSonics, Toronto, ON) with a 30 MHz transducer (RMV-707B: 55 µm axial resolution, 115 µm lateral resolution, focal length of 12.7 mm, centre frequency of 25 MHz as indicated by manufacturer) (20–22,32–40). A motorized scan stage (VisualSonics, Toronto, ON) was used to acquire volumetric data at a step size of 0.2 mm. The focal zone was placed slightly below the centre of the middle volumetric 2D plane. Power Doppler data were collected with the following optimized settings: a clutter-filter cut-off of 1.0 mm/s, a scan speed of 0.8 mm/s, a pulse repetition frequency of 4 kHz, a power Doppler gain of 20 dB, and a frame rate of ~10 fps. The reconstructed 3D images can be utilized to quantify vascular density and average blood vessel sizes and to provide information about the vascular structure, distribution and branching in tumours (6, 21, 39, 41). For this study, analysis of Power Doppler data was conducted using in-house developed software in MATLAB (R2011b, MathWorks, Natick, MA). The vascularity index (VI) was computed from the power Doppler images by obtaining the volume of all colored objects (colored pixels) over the volume of the selected regions of interest (ROI) per whole tumour. A relative vascularity index was used to assess overall vascular response to therapy, computed by dividing the VI at a given time (VI_h, where h can be 3 h, 24 h, or 72 h) by the VI at 0 h (VI_0) as below:

$$\text{Relative VI} = (VI_h / VI_0) \times 100 - 100 \quad (1)$$

To minimize any artefacts that might arise from vibrations in the room, animals were placed on an anti-vibration stage (Thor Labs, Ely, UK). Tumours were imaged immediately prior to administering any treatment ("pre-treatment" imaging), and at 3 h, 24 h or 72 h after treatment ("post-treatment" imaging).

Raw radiofrequency (RF) data was recorded digitally (sampled at 420 MHz) with a 12-bit dynamic range using a VEVO770 (RMV 707b; VisualSonics, Toronto, Canada) to assess acute tumour response (cell death) using QUS spectroscopy methods (42). QUS generally refers to methodologies that examine frequency-dependent backscatter and power spectrum-based statistical estimates of backscatter contributors from RF raw data (i.e., before envelope detection, log amplification, and B-mode image formation) to characterize tissue acoustic properties (43, 44). Parameters can be obtained from a linear-regression fit to the power spectrum of the signal that are related to the effective scatterer size and/or the acoustic scatterer concentration of the imaged tissue (45–47). Various studies have demonstrated that these parameters are sensitive to subtle micro-structural characteristics and alterations occurring in tissue due to biological responses to cancer treatment such as cell death (23,25,48–54). Parameters obtained from QUS do not rely on exogenous contrast agents, and relate to the physical and acoustic properties of tissues and underlying cells as they change due to treatment (42). QUS methods are mostly independent of machine settings due to normalization to a reference spectrum acquired at each imaging session. This is a desirable attribute that makes these methods more robust and advantageous over quantification using conventional B-mode imaging by eliminating a major source of uncertainty (44). Fourier-based spectroscopic analysis of ultrasound RF data was conducted on rectangular regions of interest (ROI), selected by placing the largest possible rectangular ROI within the tumour cross-sectional image without going outside of the tumour tissue itself. A total of 10 ROIs on separate 2D planes were selected for each tumour volume, at each time point. The power spectrum was estimated by taking the square of the magnitude of the fast Fourier transform (FFT) of the Hamming-gated RF echo segment $e_s(t, x_i)$, as a function of time (t) and lateral position (x_i) for each scan line in each ROI. An average power spectrum was obtained for each of the ROIs. All data was normalized using previously validated methods that rely on a reference calibration spectrum $e_p(t, x_i)$ (obtained from a flat plexi glass echo segment) to determine quantitative spectral parameters. The normalization process reduces the influence of system

properties and instrument settings on spectroscopic analysis. The power spectrum for each ROI can hence be obtained from:

$$S(f) = \frac{\sum_{i=M}^{N} \left| FFT(e_s(t, x_i)) \right|^2}{\sum_{i=M}^{N} \left| FFT(e_p(t, x_i)) \right|^2} \quad (2)$$

where $i = M, M + 1, \ldots, N$ RF lines in the ROI window. Quantitative spectral parameters were derived from a linear-regression approximation (in logarithmic scale) within a -6 dB window to the normalized power spectrum. Parameters of interest include the spectral slope (slope of line-approximation; SS), the 0-MHz spectral intercept (y-axis intercept of line-approximation; SI), the mid-band fit (solution of line-approximation at the centre frequency of -6 dB bandwidth; MBF). These parameters are, in turn, related to the scatterer size (SI, SS), the acoustics scatterer concentration (MBF, SI), or difference in acoustic impedance between the scatterer and its surrounding medium (SI). More specifically, parameters were obtained using the following equations, where f_c is the central frequency:

$$S(f) = SS \times f + SI \quad (3)$$

$$MBF = S(f_c) \quad (4)$$

The MBF parameter has been demonstrated to be the most representative of treatment response in pre-clinical studies, with good correlation to cell death (52,53). As a result, this study primarily focused on this parameter. In addition, spatial parametric images of MBF were also generated by displaying the results of a sliding window analysis on a pixel-by-pixel basis within the ROI using a Hamming function. Parametric images were produced using a sliding window with a time-bandwidth product of ~7.

Immunohistochemistry

Animals were euthanized by cervical dislocation and tumours were excised for immunohistological staining. Tumours were sectioned in halves; one half was fixed in formalin and the other was placed in an optical gel and flash frozen with liquid nitrogen. Formalin-fixed tumour sections were used for staining, while flash-frozen sections were kept as backup or for potential future use. The formalin fixed sections were first stored up to 2 days in room temperature and then moved to a 90% ethanol solution and stored at 4°C for up to 5 additional days. These specimens were sectioned into 5 µm thick slices and mounted on glass slides for staining. From each tumour, 3 sections were stained with hematoxylin and eosin (H&E), *in situ* end labeling (ISEL) or cluster of differentiation 31 (CD31). Staining with H&E was used for general surveying of tumour morphological alterations following therapy and was not quantified. Staining with ISEL was quantified by computing a ratio of ISEL stained areas to whole tumour cross-sectional area, resulting in a percent cell death index. This was carried-out using a custom MATLAB (The MathWorks, Natick, MA) routine, which allows the user to compute the number of brown pixels (ISEL-stained) over the total number of pixels per whole segmented tumour cross-section in a digitized histology slide (7,27,31). Endothelial-specific CD31 staining was used to quantify micro-vascular densities (MVD) and to complement power Doppler findings. This was done by counting the number of stained blood vessels in 4-5 fields of view (vessels per 0.623 mm^2) under a 20× objective lens, as described in (55). All immunohistology quantification was performed by the same person for consistency.

Statistical Analysis

Two-way analysis of variance (ANOVA) on quantitative parameters was carried-out to assess treatment interactions. More specifically, ANOVA was used to test if radiation dose has the same effect on each of the parameters at all USMB doses. If no interaction was found, testing was conducted to determine if radiation or USMB dose affects results independently. Quantitative parameters include the power Doppler VI; the QUS MBF, SS and SI; the CD31 MVD; the ISEL percent cell death. In addition, pairwise multiple comparisons were performed using Tukey's Honest Significant Difference Procedure to test for significance between each condition and the control condition (0 Gy and No USMB) at 3 h, 24 h or 72 h (56, 57); statistical significances ($p < 0.05$) are indicated by * directly in figures. Correlations between quantitative parameters were done with the Spearman correlation coefficient (r) and the coefficient of determination (R^2 - from best-fit via linear or quadratic regression). All statistical analyses were done using MATLAB (The MathWorks, Natick, MA) and GraphPad Prism (GraphPad Software, La Jolla, CA).

Results

Representative maximum intensity projection of power Doppler tumour blood flow at 24 h after the indicated treatment, rendered from volumetrically-acquired power Doppler ultrasound images, qualitatively demonstrated a decrease in power Doppler signal following a single dose of 2 Gy radiation combined with the high dose USMB therapy (Figure 2-top row). Figure 2 also exhibits representative QUS-ROIs overlaid on 2D B-mode

images obtained from the volumetric data (second row). The third row (Figure 2) exhibits representative QUS-MBF parametric maps generated within the specified ROI at 24 h after the indicated treatment. Images qualitatively demonstrate an increase in the MBF intensity by 24 h in tumours treated with radiation and USMB.

Quantified relative VI values are plotted in Figure 3A. We observed that treatments with USMB alone (0 Gy, leftmost panel) had minimal effect on the VI. A slight increase in VI signal was observed at 72 h. Treatments with radiation alone (No USMB and 2 or 8 Gy) caused the VI to decrease at all three times. A relative VI average significant decrease of up to 31% was noted in animals treated with the 8 Gy radiation dose as early as 3 h after treatment. When ultrasound-stimulated microbubbles (Low and High) were delivered in conjunction with radiotherapy, a relative VI decrease of up to 46% was noted at the 2 Gy and 8 Gy doses, respectively. This was observed as early at 3 h for 2 Gy with Low USMB. At 24 h, only combinations of low ($p < 0.05$) and high ($p < 0.01$) USMB with 2 Gy or 8 Gy radiation were found to exhibit statistically significant effects. Finally, we noted tissue re-perfusion (increase in the power Doppler VI relative to baseline) when by 72 h for all combined treatments. ANOVA of the relative power Doppler VI indicated a significant synergistic interaction between radiation and USMB at 24 h only ($p < 0.01$).

The changes in MBF values from "pre-" to "post-treatment" scans (ΔMBF) at different times are quantified and presented in Figure 3B as a function of treatment condition and time. Results suggest some increases in the MBF parameter following treatment with USMB alone. Treatments with 2 Gy radiation combined with microbubble treatments at the low USMB concentration exhibited a similar response to delivering 8 Gy radiation alone. An increase of up to 5 dBr by 72 h was noted in animals treated with 2 Gy

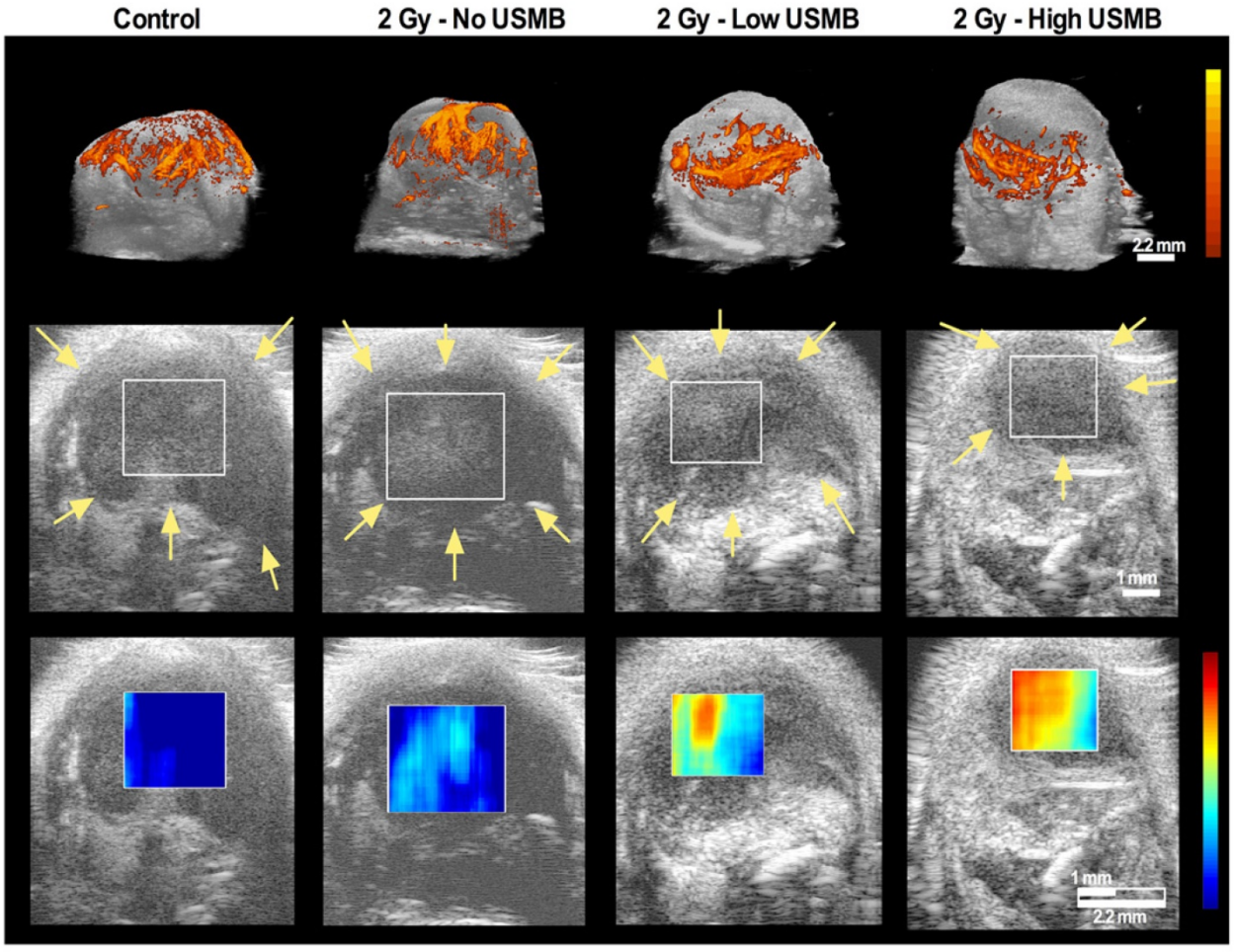

Figure 2. Top row exhibits volumetric maximum intensity projections of tumour power Doppler signal for a control tumour at 24 h, as well as following 2 Gy alone, or in combination with Low USMB and High USMB (all at 24 h). Results qualitatively demonstrate a decrease in power Doppler signal as a function of treatment. The second row exhibits 2D B-mode images of a single plain in the center of a tumour volume with a rectangular overlay as a representative ROI used for QUS analysis. Images are of post-treated tumours. The third row exhibits parametric map overlays of the MBF in the selected ROIs. One can observe an increase in signal as a function of treatment. Color legend bars encompass 40 dB for power Doppler and 12 dBr for the MBF parametric map images. Yellow arrows indicate the tumour tissue-skin boundary. Scale bars denote 2.2 mm for power Doppler and 1 mm for Bmode/QUS parametric map.

radiation and a high USMB dose. In tumours treated with 8 Gy alone, we noted an MBF increase of ~1-2 dBr by 24 h and 72 h. The addition of microbubbles to single 8 Gy radiation doses enhanced the ΔMBF by 24 h (~ 4 dbr for Low and ~ 5 dBr for High) and 72 h (> 5 dBr for High). We have also extracted the MBF, SS and SI. Results for these parameters are presented in Supplementary Figure S3. No statistically significant interactions were noted between radiation and USMB at any of the time-points in the QUS-MBF parameter. Radiation dose significantly affected MBF values at all time-points ($p < 0.01$ at 3 h; $p < 0.001$ at 24 h; $p = 0.001$ at 72 h). Similarly, USMB dose affected MBF results at all time points ($p = 0.01$ at 3 h; $p < 0.01$ at 24 h; $p < 0.0001$ at 72 h).

Figure 4A exhibits representative images of ISEL (top) and CD31 (bottom) stained tumour cross-sections at 24 h, respectively. A qualitative response was observed in treated versus non-treated tumours. Figure 4B presents quantified percent cell death obtained from ISEL staining. USMB therapy delivered alone had no observable effect on cell death. Combination treatments of radiation and USMB resulted in a significant increase in the cell death index when compared with the corresponding radiation only conditions, for each of the experimental times. Quantification of cell death from ISEL staining was in general agreement with qualitative findings. The use of a low USMB dose with a single dose of 8 Gy radiation resulted in an increase in cell death relative to 8 Gy alone at 24 h. A similar enhancement trend in cell death was observed in other conditions with combined treatments at 24 h and 72 h. However, through this analysis, we noted minimal cell death at the 3 h time. We also noted up to 200% greater amounts of cell death at 24 h and 72 h, in comparison to quantified cell death at 3 h. A statistically significant interaction was noted between radiation and USMB for ISEL quantification at 72 h ($p = 0.04$).

Vascular CD31 staining was used to assess micro-vascular response and to confirm power Doppler results. Representative images of tumour cross sections obtained at 24 h after treatment are shown in Figure 4A. Quantified CD31 staining based on the MVD method (Figure 4C) showed negligible effects when USMB were used alone; over a 72 h period, we observed a marginal increase in MVD (< 20%). Additionally, radiation alone (no USMB) caused a decrease in MVD of > 10-20%. When USMB were delivered in conjunction with radiotherapy, we observed a decrease in the MVD greater than 50% of the original values. We also noted an average MVD decrease of ~45% for combined USMB and 2 Gy irradiation at 24 h. Similarly, at 72 h, the use of USMB resulted in a decrease in the MVD compared to radiation alone. In addition, it was observed that MVD values vary minimally between the 24 h and 72 h time endpoints, reminiscent of results obtained from power Doppler analysis. Statistically significant interactions were observed at 72 h ($p = 0.02$). Radiation dose significantly affected CD31 MVD at 3 h and 24 h ($p = 0.03$ and $p < 0.01$, respectively); USMB dose affected CD31 MVD results at 24 h ($p = 0.03$).

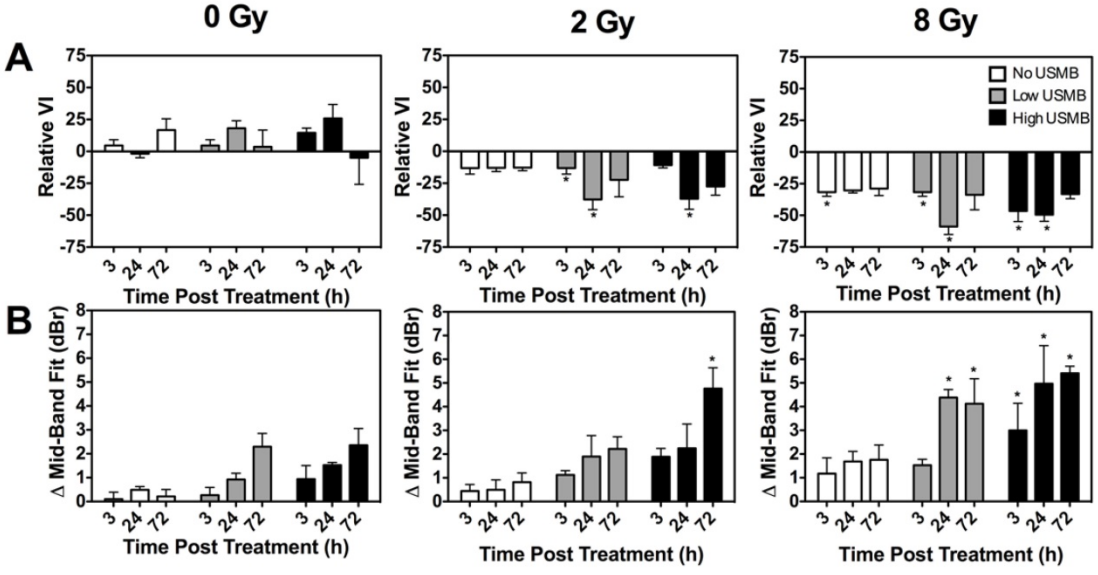

Figure 3. (A) Quantified power Doppler vascularity index (VI) at 3 h, 24 h and 72 h for control, single doses of 2 Gy or 8 Gy radiation, low and high concentration of USMB, and combined treatment permutations. The graphs exhibit the relative change of Doppler signal represented as the relative VI. There is a decrease in the VI for combined microbubble and radiation treated tumours when compared with the radiation only conditions, entailing an enhanced radiotherapy effect with the use of microbubbles. (B) Quantified MBF for the same treatment conditions. Similar to power Doppler results, we note a greater increase in the MBF QUS parameter in animals treated with radiation and microbubbles, in comparison to those treated with radiation or microbubbles alone. Significance is indicated by * for $p < 0.05$. All conditions are compared to the control condition (0 Gy and Nil microbubbles of the corresponding time points).

In Figure 5A, correlations of MVD values to the relative VI at the 3 h, 24 h and 72 h times are presented. Results suggest that the best fit within the 95% confidence interval occurs at the 24 h and 72 h times, with R^2 values of 0.8 and 0.6, respectively. Spearman correlation indicated significant correlations at 24 h and 72 h ($p = 0.15$ at 3 h; $p < 0.01$ at 24 h; $p = 0.01$ at 72 h). Similarly, Figure 5B exhibits correlations of the cell death (ISEL) to the **Δ**MBF at the 3 h, 24 h and 72 h times. From these, excellent correlative fits within the 95% confidence interval (with an $R^2 > 0.8$) were observed at the 24 h and 72 h times. Spearman correlation indicated a significant correlation at 24 h and 72 h ($p = 0.09$ at 3 h; $p < 0.01$ at 24 h; $p < 0.01$ at 72 h).

In Figure 6, correlations between the acute tumour vascular response and acute tumour response (cell death) are presented. Figure 6A and 6B exhibit correlations between the relative VI and the ΔMBF with a linear regression fit, respectively. An R^2 of 0.4-0.5 was noted in the linear regression analysis. Spearman correlation indicates a significant correlation at 3 h and 24 h ($p = 0.04$ at 3 h; $p = 0.01$ at 24 h; $p = 0.09$ at 72 h). In Figure 6B, presented are first order correlations between CD31 and ISEL stained quantified results. Spearman correlation indicated a significant correlation at 24 h and 72 h ($p = 0.06$ at 3 h; $p < 0.01$ at 24 h; $p = 0.05$ at 72 h).

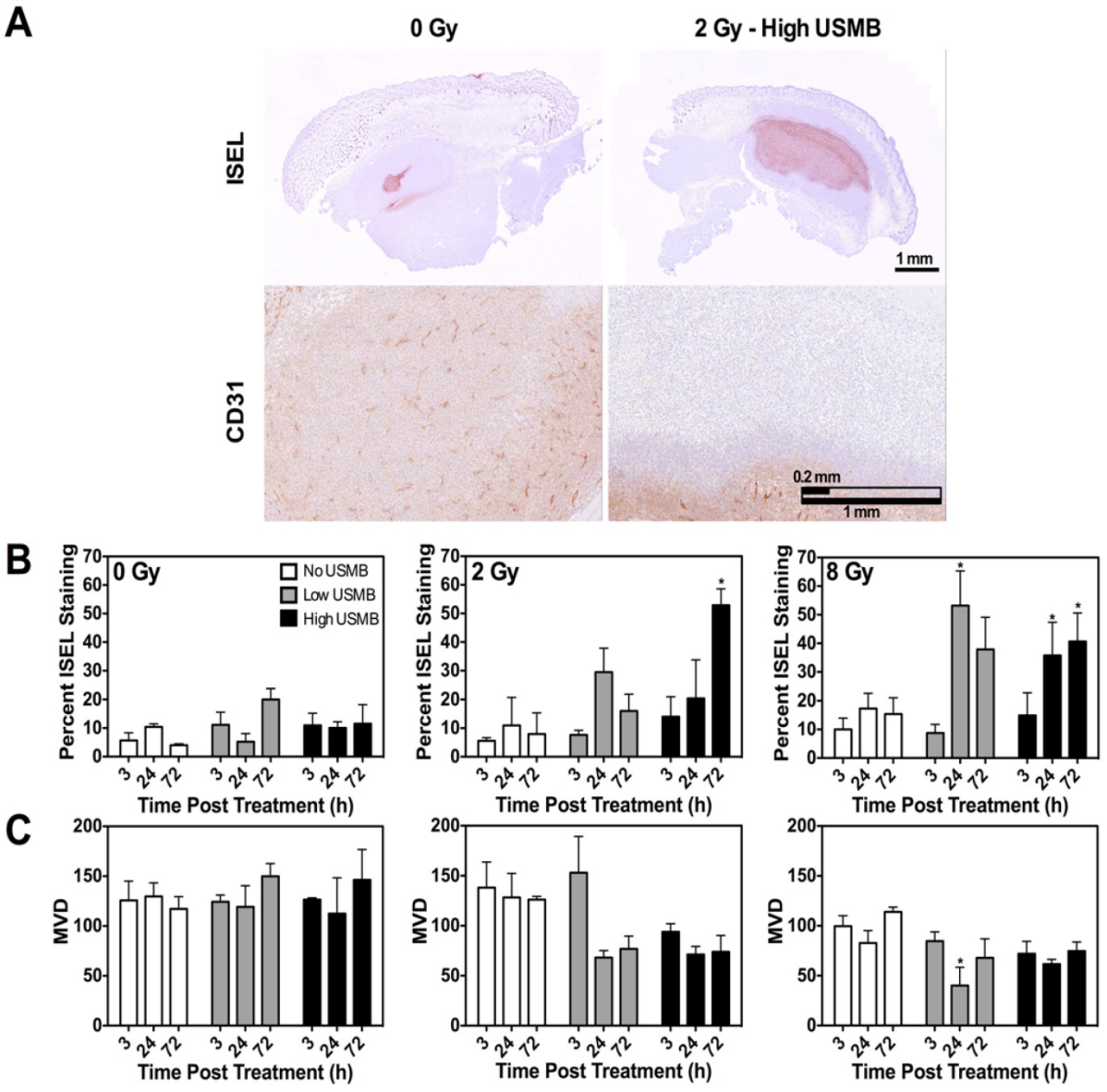

Figure 4. (A) Representative images of ISEL (top) and CD31 (bottom) stained tumour cross-sections obtained at 24 h post-treatment. Panel demonstrates qualitative increases in cell death and decreases in the microvasculature density in treatment when comparing the control and treated conditions. The scale bars denote 1mm and 0.2 mm in ISEL and CD31, respectively. (B) Quantified ISEL stained tumour cross-sections as a gold standard measurement of tumour cell death. We note an overall increase in cell death in animals treated with the combination treatments. (C) Quantified CD31 stained tumour cross sections, expressed as the MVD. Results confirm a decrease in vascularity in animals receiving combined therapy. Significance is indicated by * for $p < 0.05$. All conditions are compared to the control condition (0 Gy and Nil microbubbles of the corresponding time points).

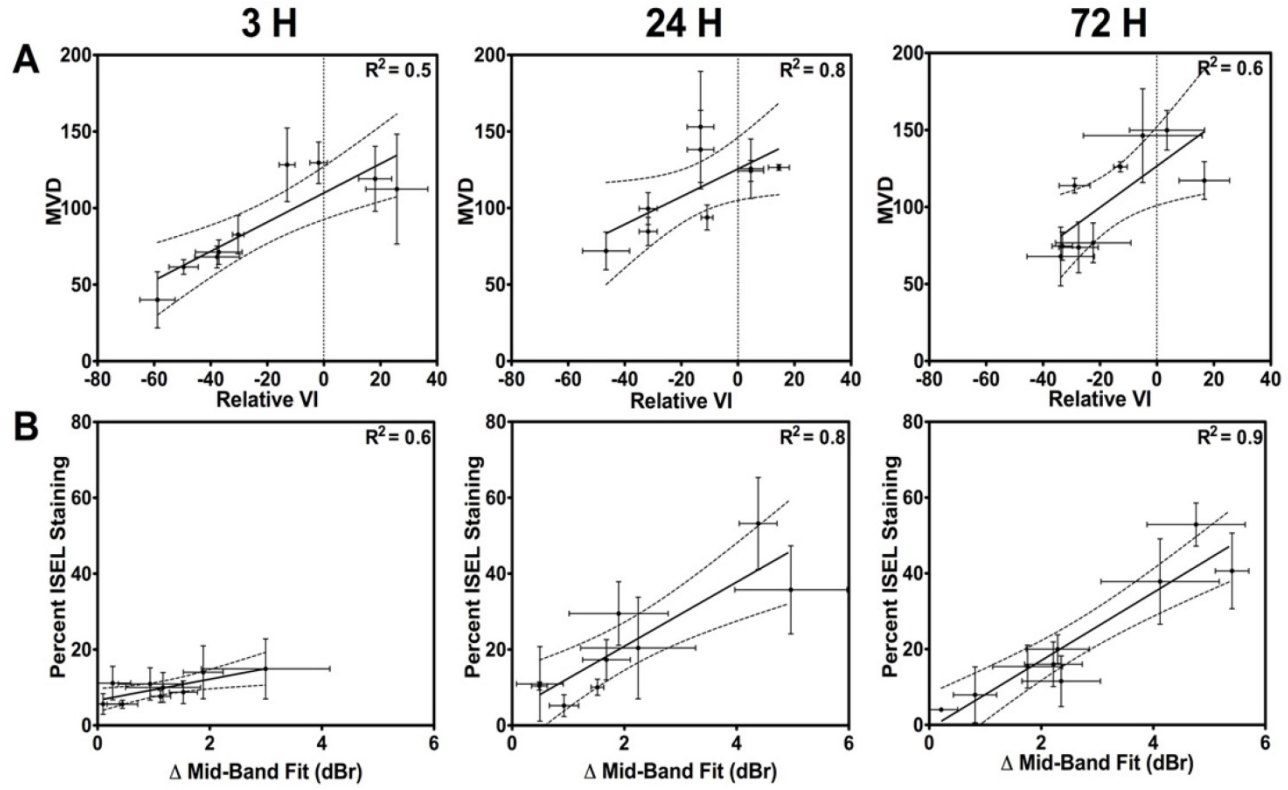

Figure 5. (A) Correlations between quantified CD31 results and the power Doppler VI parameter. Good correlations are noted at 24 h and 72 h. (B) Correlations between quantified ISEL results and the QUS-MBF parameter. A good correlative agreement is noted, especially at 24 h and 72 h. These confirm ultrasound-based link to gold standard histology.

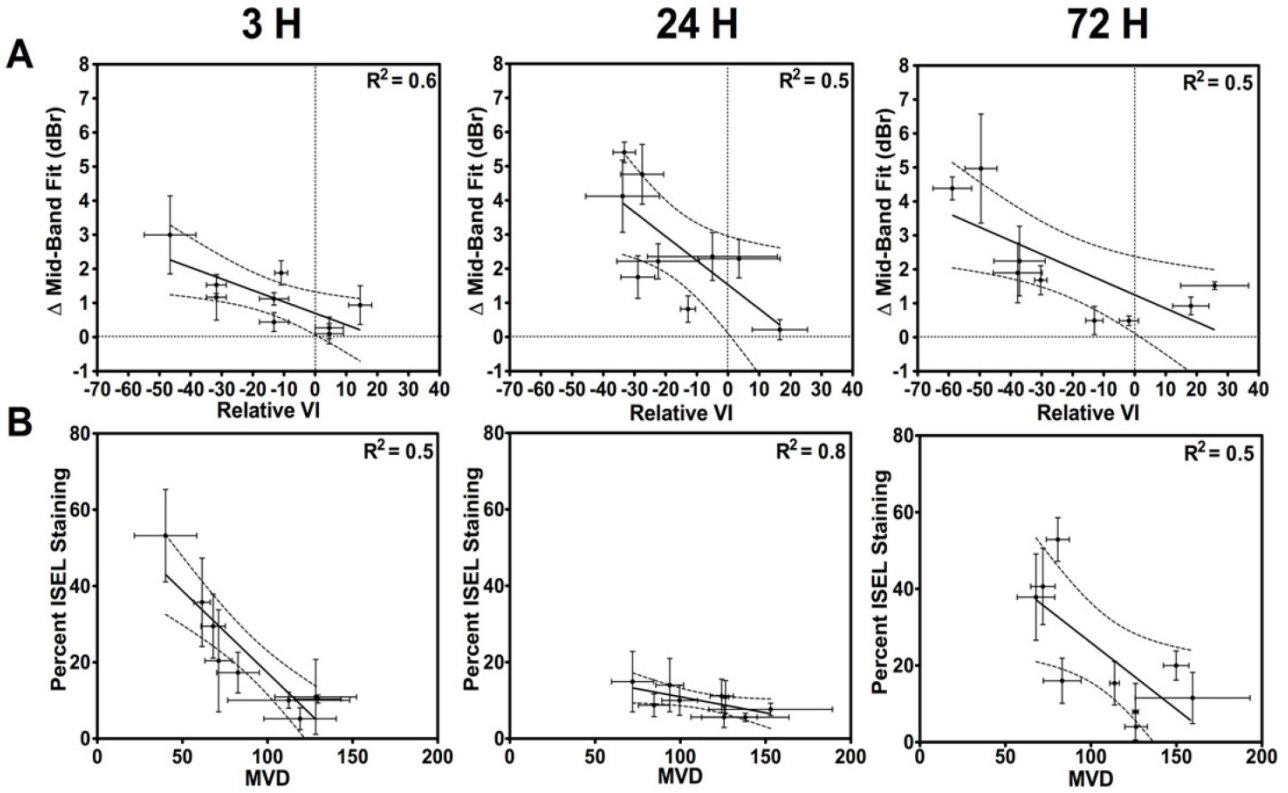

Figure 6. (A) First-order correlations between the VI and the MBF. (B) Correlations between the percent cell death (ISEL) and the MVD (CD31). Correlations with an $R^2 > 0.7$ are found at 24 h.

Discussion

In this study, longitudinal vascular and tumour responses to radiation and USMB were investigated using *in vivo* ultrasound imaging. The findings here support the use of ultrasound in radiation studies as a diagnostic modality (to characterize vascular and tumour response effects), as well as a therapeutic modality (to complement radiation effects). We demonstrated, for the first time, a relationship between rapid vascular disruption and short-term tumour cell death, suggesting that acute tumour damage is a direct product of tumour vascular shut-down. Good correlative agreement was found between power Doppler and QUS results, as well as between CD31 and ISEL staining results ($p < 0.05$). Observations indicated that the extent of vascular response (found with power Doppler and CD31) is significantly ($p < 0.05$; Spearman correlation) linked to acute tumour responses (found with QUS and ISEL). This validates previous findings that acute tumour cell death is, at least in part, regulated by vascular disruption (5). In addition, findings reinforce that microbubbles, stimulated with ultrasound and administered immediately before radiation therapy, significantly enhance the tumour response, and that this enhanced radio-response is linked to an acute vascular response occurring within hours after treatment administration.

To date, substantive evidence suggests that tumour blood vessels act to regulate tumour responses to radiotherapy (5, 8, 9, 58–61), challenging the canonical notion that this response is primarily dependent on an inherent radiosensitivity of clonogenic tumour cancer cells. In 2003, Folkman and Camphausen (3) speculated on the question: "What does radiotherapy do to endothelial cells?" Concurrently, researchers were prompted to query radiation-induced effects on endothelial cells, and whether vascular dysfunction could be targeted to regulate tumour response to radiation therapy at high doses. It was suggested that if the microvasculature is the primary target of radiation in the intestine, as posited earlier by Paris and colleagues (62), and if damage to epithelial stem cell is a secondary event, then such a relationship may hold even in tumours where endothelial cells also support surrounding tumour cells. Reports of differing tumour radiosensitivities *in vivo* and *in vitro* could be explained by the presence of host-derived supporting cells (i.e., endothelial cells). One could also take advantage of increased tumour endothelial cell radiosensitivity (compared to normal endothelial cells) to better target tumours (63). In 2003, Garcia-Barros et al. (5) published results supporting high-dose (>8-10 Gy and up to 22 Gy) radiation primarily targeting endothelial cells as regulators of tumour response to radiotherapy. A series of publications by various groups have since repeatedly confirmed these findings and advanced our knowledge of endothelial cell radiobiology, particularly at high radiation doses (6,18,64,65).

The resulting question from this body of work is: are tumour responses to radiation regulated by the inherent radiosensitivity of the tumour cells or by the host derived stroma? Our study, here, using *in vivo* imaging, supports the idea that tumour responses in the form of rapid cell death are directly linked to acute vascular disruption. Methods presented here establish a foundation for future investigations in understanding this complex relationship longitudinally (over longer times), as a function of baseline imaging biomarkers, and as a function of treatment response. Recognizing that the role of blood vessels in regulating tumour response to radiation response is likely complicated, a paradigm shift is underway, which gives a more prominent role to the tumour stroma and the endothelium component in radiation planning and delivery. While various newly developed vascular targeting agents have been demonstrated to act synergistically with radiation therapy to target tumour blood vessels, in this work, we use mechano-acoustic targeting of tumour blood vessels to study the relationship between acute tumour vascular disruption and tumour cell death (18).

The mechano-acoustic therapeutic strategy described here, which utilizes USMB, embodies a paradigm shift in radiation-based tumour targeting. The methodology proposed enhances radiation effects above and beyond currently existing agents that target tumour vasculature alone; massive cell death that is triggered by ultrasound-microbubbles surpasses transient hypoxia with subtle radiobiological effects, resulting in complete tumour destruction and inevitable cell death. Several published studies have investigated the mechanism of USMB-based radiosensitization, suggesting it is related to ceramide transduction following endothelial membrane stimulation (12,18,66). More specifically, the working mechanistic model is that while high doses (> 8 Gy) of radiation activate sufficient quantities of ceramide to induce endothelial cell death, radiation doses lower than 2-6 Gy do not release enough ceramide to activate ceramide-induced cell death(3,8). Similarly, while ceramide is released following USMB treatments, the amount is not sufficient to activate rapid and extensive cell death for vascular shut-down when used alone(11,12,30). In contrast, combining radiation

(low or high dose) with USMB releases enough ceramide to pass a threshold that results in extensive tumour endothelial cell death and vascular shut-down, even at 2 Gy. In this mechanism, the radiation effect is converted from tumour-cell DNA damage alone, to additional vessel destruction and tumour apoptosis and necrosis. The concern that such vessel destruction may inhibit further radiotherapy is obviated by the complete cell death detected histologically (anoxic or ischemic-like) and the superior cure rates seen experimentally. In this type of ultrasound treatment, microbubbles are administered intravenously and act on blood vessel endothelial cells only. Tumour selectivity and a therapeutic ratio is obtained by focusing the ultrasound beam only on the tumour. Thus, the development of a new and more potent body of high-dose radiobiology incorporating stromal effects and other cell death pathways (i.e., via the membrane and ceramide), as well as mechanical radiosensitizers, is on the horizon (64). To that end, all USMB exposures in this work used treatment parameters, timing and set-ups that have previously been demonstrated to yield radiosensitization effects. However, there may be additional parameters and conditions that could be more optimal and efficient at delivering USMB treatment with radiation. These should be the topic of future research.

This work contributes to this evidence directly by presenting *in vivo* imaging results indicating that tumour cell death is directly linked to acute vascular disruption. These results demonstrated that USMB treatment administered alone had minimal acute effects on tumour vasculature and tumour cell death. Tumours treated with radiation only resulted in a small, but dose-dependent VI decrease. Treatments with 2 Gy alone caused a non-significant, but rapid vascular shutdown, which was sustained for up to 72 h. A similar response was not observed in CD31-stained tumour cross sections, indicating that the response was predominantly reflected in larger vessels detectable with power Doppler ultrasound. Single 8 Gy doses caused a substantial decrease in tumour vasculature in both CD31 staining and power Doppler results. This was in agreement with previous findings (7). Average decreases of up to ~ 25% were noted by 3 h after treatment and remained as such for 24 h. However, by 72 h, results suggest a potential re-vascularization/re-perfusion effect reminiscent of previously reported tissue reperfusions ('vascular rebounds') following anti-vascular treatments (67,68). Similarly, the QUS MBF-parameter increased with VI decrease. Indeed, the effect was inversely proportional to the power Doppler VI parameter, suggesting that a greater vascular disruption will result in acute tumour response (cell death).

Tumours receiving combined USMB and radiation treatments resulted in the greatest vascular and tumour response at all three time points following treatment delivery. Flow signals in power Doppler volumetric images decreased within 3 h after initiation of treatment in animals receiving any possible permutation of combined radiation and microbubble doses. Microbubble-based enhancement of radiation therapy appeared to be the most effective when combined with 8 Gy doses of radiation. Here, the VI decreased by up to 50% at 3 h following treatment for both high and low microbubble doses. Vascular disruption was sustained at the 50% level for up to 72 h. Similarly, the QUS-MBF parameter significantly increased by 3 h (by ~2-4 dB), matching the 24 h response of 8 Gy treatments delivered alone. Results suggest that the vascular effect is intense, causing a detectable tumour response and tumour cell death almost simultaneously, reminiscent of ischemic-like conditions where tissue viability is compromised within seconds of blocked oxygen delivery. These results illustrate the potential of USMB therapies to improve radiation-based vascular targeting strategies, and the need for *in vivo* vascular imaging to provide evidence for vascular effect considerations during cancer treatment planning and administration.

Quantified ISEL-based cell death in tumour cross sections demonstrated the regulating role of vasculature in tumour response to radiation therapy. These results indicated general increases in cell death as a function of increasing radiation doses augmented with microbubble therapy, as previously reported (12,15,19,52). Here, an overall increase in cell death was observed in the combined treatment conditions when compared to radiation alone. These observations were made at both 24 h and 72 h. However, minimal effects were observed at 3 h after treatment, suggesting that vascular effects may take up to 24 h to manifest into cell death. Immunohistochemical staining was used primarily as gold standard to confirm ultrasound results, where ISEL results were correlated to the QUS MBF parameter and CD31 results were correlated with the power Doppler VI result. The percent cell death quantified from ISEL results and the QUS MBF parameter had a proportional relationship and were in good correlative agreement at the 24 h and 72 h times. Similarly, we noted a good correlative agreement and proportionality between the power Doppler VI and the CD31-based MVD at 24 h and 72 h. The relationship between the vascular and tumour responses was also investigated. A qualitative direct link was first noted between the observed vascular

response and tumour cell death. We noted (Figure 6) that when radiation was delivered alone, or in combination with microbubbles, a weak (R^2 = 0.4-0.5), inversely proportional linear relationship was present between the ΔMBF and the relative VI. We also observed an inversely proportional linear relationship between CD31 and ISEL results, with an R^2 of 0.5-0.8 at the 24 h and 72 h time points. Finally, we found small correlations between ISEL and ΔMBF at 3 h (Figure 5B; R^2 of 0.6); this is much weaker than correlations found between the same parameters at 24 h and 72 h (up to R^2 of 0.9). At 3 h, it is unlikely that biological apoptotic cell death, detectable with ISEL, has occurred. Thus, ISEL quantification should be minimal, while structural changes in the tissue may have already occurred following extreme treatments – hence, the correlation is the weakest of the three in Figure 5B. The ISEL values may instead be related to pre-existing tumour cell death at baseline or other forms of rapid/acute cell death, which, while very small, results in a small correlation (R^2 = 0.6). This may also explain the effect observed in Figure 6B, where ISEL is correlated to MVD, where an acute decrease in vasculature is observed, but not cell death. Overall, the effects may be more complex (especially at 3 h) and future studies should include baseline histopathology and other confirmatory *in vivo* pre-clinical imaging. Taken together, observations made here suggest that blood vessels play a key role in regulating the tumour microenvironment, as previously reported (69). More importantly, longitudinal imaging methodology to characterize response of different tumour components (i.e. tumour cell death vs. tumour perfusion) simultaneously and study their relationship could be used beyond the specific USMB and XRT treatments used here. These could be utilized as multi-parametric methods to optimize other combinatory treatment regimens (increasingly common in cancer therapy) to optimize timing and dosing effects, or to identify multi-parametric imaging biomarkers.

Whereas the results from the experiments presented here demonstrate the effects of the USMB treatments in conjunction with single doses of radiation, uncertainties remain with respect to the mechanisms underlying enhanced tumour responses. The results here confirm that high radiation doses invoke rapid vascular shutdown and rapid cell death, likely linked to anoxia-based effects. However, effects at low radiation doses combined with the USMB are likely linked to other radiation or microbubble-based tumour damage. Our results contribute to the growing body of literature validating the efficacy of QUS techniques for treatment monitoring in preclinical and clinical applications (26,53,70,71). However, future studies should aim to quantify RF-based biomarkers using more robust parameters such as the effective scatterer size and concentration, which have been demonstrated to be more closely related to principle physical properties of the tissue being imaged. Furthermore, the calculations of these parameters include attenuation correction methods to compensate for errors arising from tissue signal attenuation (44, 48, 72).

Ultrasound is a relatively inexpensive and accessible medical imaging modality compared to other imaging technologies proposed for cancer treatment monitoring such as positron emission tomography (PET), single-photon emission computed tomography (SPECT), and magnetic resonance imaging (MRI) (70,73). We have demonstrated the value of quantitative ultrasound imaging as a tool for pre-clinical and clinical characterization of multiple biomarkers associated with cancer tissue responses to treatment. Most importantly, our findings lay the groundwork for future investigations of the mechanism of tumour and tumour vascular response in the context of different single or combined cancer treatment regimens. These results support the ongoing paradigm shift towards vascular-based regulation of tumour response to cancer therapies (in particular radiation therapy), and, more significantly, present a foundational case for the use of ultrasound microbubbles as vasculature radiosensitizers to enhance radiotherapy. Finally, our results indicated a proportional relationship between acute tumour cell death and radiation-induced vascular effects using *in vivo* longitudinal imaging. These results are a stepping-stone towards developing more accurate theoretical models of radiation effects on tumour tissue that incorporate vascular effects, and validate ultrasound as a theranostic tool in radiation oncology.

Abbreviations

USMB: ultrasound-stimulated microbubbles; QUS: quantitative ultrasound; ISEL: *in situ* end labelling; CD31: cluster of differentiation 31; ASMase: acid-sphigomyelinase; PBS: phosphate buffered saline; SSD: source to surface distance; VI: vascularity index; ROI: region of interest; RF: radiofrequency; FFT: fast Fourier transform; SS: spectral slope; SI: 0-MHz spectral intercept; MBF: mid-band fit; H&E: hematoxylin and eosin; MVD: micro-vascular densities; ANOVA: analysis of variance; PET: positron emission tomography; SPECT: single-photon emission computed tomography; MRI: magnetic resonance tomography.

Supplementary Material

Supplementary figures; details about the treatment system set-up, the ultrasound field, and additional results of the extracted ultrasound parameters.
http://www.thno.org/v08p0314s1.pdf

Acknowledgements

The fibrosarcoma cell line (MCA-129) was obtained from Drs. Zvi Fuks and Richard Kolesnick's laboratories at the Memorial Sloan-Kettering Institute for Cancer Research, as were the initial colony forming mice used in this research. G.J. Czarnota is supported by a James and Mary Davie University of Toronto Chair in Breast Cancer Imaging and Ablation.

Funding

This work was supported by the Canadian Cancer Society Research Institute (CCSRI), Natural Science and Engineering Research Council (NSERC), and the Terry Fox Foundation.

Competing Interests

The authors have declared that no competing interest exists.

References

1. Hall EJ, Giaccia AJ. Radiobiology for the radiologist. New York: Lippincott Williams & Wilkins; 2006. 546 p.
2. Lehnert S. Biomolecular action of ionizing radiation. New York: Taylor & Francis; 2007. 527 p.
3. Folkman J, Camphausen K. What does radiotherapy do to endothelial cells? Science. American Association for the Advancement of Science; 2001 Jul 13;293(5528):227–8.
4. Kolesnick R, Fuks Z. Radiation and ceramide-induced apoptosis. Oncogene. 2003 Sep;22(37):5897–906.
5. Garcia-Barros M, Paris F, Cordon-Cardo C, Lyden D, Rafii S, Haimovitz-Friedman A, et al. Tumor response to radiotherapy regulated by endothelial cell apoptosis. Science. 2003 May 16;300(5622):1155–9.
6. El Kaffas A, Tran W, Czarnota GJ. Vascular strategies for enhancing tumour response to radiation therapy. Technol Cancer Res Treat. 2012;11(5):421–32.
7. El Kaffas A, Giles A, Czarnota GJ. Dose-dependent response of tumor vasculature to radiation therapy in combination with Sunitinib depicted by three-dimensional high-frequency power Doppler ultrasound. Angiogenesis. 2013 Jan 12;16(2):443–54.
8. Fuks Z, Kolesnick R. Engaging the vascular component of the tumor response. Cancer Cell. 2005 Aug;8(2):89–91.
9. García-Barros M, Thin TH, Maj J, Cordon-Cardo C, Haimovitz-Friedman A, Fuks Z, et al. Impact of stromal sensitivity on radiation response of tumors implanted in SCID hosts revisited. Cancer Res. 2010 Oct 15;70(20):8179–86.
10. Truman JP, Garcia-Barros M, Obeid LM, Hannun YA. Evolving concepts in cancer therapy through targeting sphingolipid metabolism. Biochim Biophys Acta - Mol Cell Biol Lipids. Elsevier B.V.; 2014 Dec 30;1841(8):1174–88.
11. Al-Mahrouki A, Karshafian R, Giles A, Czarnota GJ. Bioeffects of ultrasound-stimulated microbubbles on endothelial cells: gene expression changes associated with radiation enhancement in vitro. Ultrasound Med Biol. 2012 Nov;38(11):1958–69.
12. Czarnota GJ, Karshafian R, Burns PN, Wong S, Al Mahrouki A, Lee JW, et al. Tumor radiation response enhancement by acoustical stimulation of the vasculature. Proc Natl Acad Sci. 2012 Jul 24;109(30):E2033–41.
13. Truman J-P, García-Barros M, Kaag M, Hambardzumyan D, Stancevic B, Chan M, et al. Endothelial membrane remodeling is obligate for anti-angiogenic radiosensitization during tumor radiosurgery. PLoS One. 2010 Jan;5(8):e12310.
14. El Kaffas A, Nofiele J, Giles A, Cho S, Liu SK, Czarnota GJ. Dll4-notch signalling blockade synergizes combined ultrasound-stimulated microbubble and radiation therapy in human colon cancer xenografts. PLoS One. 2014;9(4):e93888.
15. Kim HC, Al-Mahrouki A, Gorjizadeh A, Karshafian R, Czarnota GJ. Effects of Biophysical Parameters in Enhancing Radiation Responses of Prostate Tumors with Ultrasound-Stimulated Microbubbles. Ultrasound Med Biol. 2013 Aug 30;39(8):1376–87.
16. Kwok SJJ, El Kaffas A, Lai P, Al Mahrouki A, Lee J, Iradji S, et al. Ultrasound-mediated microbubble enhancement of radiation therapy studied using three-dimensional high-frequency power Doppler ultrasound. Ultrasound Med Biol. 2013 Nov 28;39(11):1983–90.
17. Qin S, Caskey CF, Ferrara KW. Ultrasound contrast microbubbles in imaging and therapy: physical principles and engineering. Phys Med Biol. 2009;54(6):R27–57.
18. El Kaffas A, Czarnota GJ. Biomechanical effects of microbubbles: from radiosensitization to cell death. Future Oncol. Future Medicine Ltd London, UK; 2015 Apr 25;11(7):1093–108.
19. Tran WT, Iradji S, Sofroni E, Giles A, Eddy D, Czarnota GJ. Microbubble and ultrasound radioenhancement of bladder cancer. Br J Cancer. Nature Publishing Group; 2012 Jul 24;107(3):469–76.
20. Goertz DE, Yu JL, Kerbel RS, Burns PN, Foster FS. High-frequency Doppler ultrasound monitors the effects of antivascular therapy on tumor blood flow. Cancer Res. 2002 Dec;62(22):6371–5.
21. Chen J-J, Chen J-JJ, Chiang C-S, Hong J-H, Yeh C-K. Assessment of tumor vasculature for diagnostic and therapeutic applications in a mouse model in vivo using 25-MHz power Doppler imaging. Ultrasonics. Elsevier B.V.; 2011 May 20;51(8):925–31.
22. Palmowski M, Huppert J, Hauff P, Reinhardt M, Schreiner K, Socher M a, et al. Vessel fractions in tumor xenografts depicted by flow- or contrast-sensitive three-dimensional high-frequency Doppler ultrasound respond differently to antiangiogenic treatment. Cancer Res. 2008 Sep;68(17):7042–9.
23. Vlad RM, Alajez NM, Giles A, Kolios MC, Czarnota GJ. Quantitative ultrasound characterization of cancer radiotherapy effects in vitro. Int J Radiat Oncol Biol Phys. 2008 Nov 15;72(4):1236–43.
24. Kolios MC, Czarnota GJ, Lee M, Hunt JW, Sherar MD. Ultrasonic spectral parameter characterization of apoptosis. Ultrasound Med Biol. 2002;28(5):589–97.
25. Sadeghi-Naini A, Falou O, Tadayyon H, Al-Mahrouki A, Tran W, Papanicolau N, et al. Conventional frequency ultrasonic biomarkers of cancer treatment response in vivo. Transl Oncol. 2013 Jun;6(3):234–43.
26. Sadeghi-Naini A, Papanicolau N, Falou O, Zubovits J, Dent R, Verma S, et al. Quantitative Ultrasound Evaluation of Tumor Cell Death Response in Locally Advanced Breast Cancer Patients Receiving Chemotherapy. Clin Cancer Res. 2013 Apr 15;19(8):2163–74.
27. El Kaffas A, Sadeghi-Naini A, Falou O, Tran WT, Zhou S, Hashim A, et al. Assessment of tumor response to radiation and vascular targeting therapy in mice using quantitative ultrasound spectroscopy. Med Phys. 2015;42(8):4965–73.
28. Al-Mahrouki A a, Iradji S, Tran WT, Czarnota GJ. Cellular characterization of ultrasound-stimulated microbubble radiation enhancement in a prostate cancer xenograft model. Dis Model Mech. 2014 Mar 1;7(3):363–72.
29. El Kaffas A, Nofiele J, Giles A, Cho S, Liu SK, Czarnota GJ. DLL4-notch signalling blockade synergizes combined ultrasound-stimulated microbubble and radiation therapy in human colon cancer xenografts. PLoS One. 2014;9(4):11–5.
30. Nofiele JT, Karshafian R, Furukawa M, Al Mahrouki a, Giles a, Wong S, et al. Ultrasound-activated microbubble cancer therapy: ceramide production leading to enhanced radiation effect in vitro. Technol Cancer Res Treat. 2013 Feb;12(1):53–60.
31. Karshafian R. On the permeabilisation and disruption of cell membranes by ultrasound and microbubbles. University of Toronto; 2010.
32. Chen J, Lin Y, Chiang C, Hong J, Yeh C. Characterization of Tumor Vasculature Derived from Angiogenesis and Vasculogenesis by High-frequency Three-dimensional Doppler Ultrasound. Symp A Q J Mod Foreign Lit. 2010;1:2319–22.
33. Fenster a, Downey DB, Cardinal HN. Three-dimensional ultrasound imaging. Phys Med Biol. 2001 May;46(5):R67-99.
34. El Kaffas A. An Investigation of Vascular Strategies to Augment Radiation Therapy. University of Toronto; 2014.
35. Sheng-Fang Huang, Chang Ruey-Feng, Woo Kyung Moon, Yu-Hau Lee, Chen Dar-Ren, Suri JS. Analysis of Tumor Vascularity Using Three-Dimensional Power Doppler Ultrasound Images. IEEE Trans Med Imaging. 2008 Mar;27(3):320–30.
36. Pinter SZ, Lacefield JC. Detectability of small blood vessels with high-frequency power Doppler and selection of wall filter cut-off velocity for microvascular imaging. Ultrasound Med Biol. 2009 Jul;35(7):1217–28.
37. Galván R, Mercé L, Jurado M, Mínguez J a, López-García G, Alcázar JL. Three-dimensional power Doppler angiography in endometrial cancer: correlation with tumor characteristics. Ultrasound Obstet Gynecol. 2010 Jun;35(6):723–9.
38. Lacefield J, Pinter SZ, Kim D-R, Hague MN, Chambers AF, MacDonald IC. A method to validate quantitative high-frequency power Doppler ultrasound with fluorescence in vivo video microscopy. Ultrasound Med Biol 2013;19:075080–075080.
39. Chen J-J, Fu S-Y, Chiang C-S, Hong J-H, Yeh C-K. Characterization of tumor vasculature distributions in central and peripheral regions based on Doppler ultrasound. Med Phys. 2012 Dec;39(12):7490–8.
40. Pinter SZ. Investigating vascular quantification with high-frequency power Doppler ultrasound from a signal detection perspective. University of Western Ontario; 2010.

41. Chang Y-C, Huang Y-H, Huang C-S, Chang R-F. Vascular Morphology and Tortuosity Analysis of Breast Tumor Inside and Outside Contour by 3-D Power Doppler Ultrasound. Ultrasound Med Biol. 2012:;1–11.
42. Kolios MC, Czarnota GJ. Potential use of ultrasound for the detection of cell changes in cancer treatment. Future Oncol. 2009 Dec;5(10):1527–32.
43. Czarnota GJ, Kolios MC, Abraham J, Portnoy M, Ottensmeyer FP, Hunt JW, et al. Ultrasound imaging of apoptosis: high-resolution non-invasive monitoring of programmed cell death in vitro, in situ and in vivo. Br J Cancer. 1999 Oct;81(3):520–7.
44. Oelze ML, Mamou J. Review of Quantitative Ultrasound: Envelope Statistics and Backscatter Coefficient Imaging and Contributions to Diagnostic Ultrasound. IEEE Trans Ultrason Ferroelectr Freq Control. 2016;63(2):336–51.
45. Lizzi FL, Greenebaum M, Feleppa EJ, Elbaum M, Coleman DJ. Theoretical framework for spectrum analysis in ultrasonic tissue characterization. J Acoust Soc Am. 1983 Apr;73(4):1366–73.
46. Lizzi FL, Astor M, Liu T, Deng C, Coleman DJ, Silverman RH. Ultrasonic spectrum analysis for tissue assays and therapy evaluation. Int J Imaging Syst Technol. 1997;8(1):3–10.
47. Lizzi FL, Feleppa EJ, Kaisar Alam S, Deng CX. Ultrasonic spectrum analysis for tissue evaluation. Pattern Recognit Lett. 2003 Feb;24(4–5):637–58.
48. Oelze ML, O'Brien WD, Blue JP, Zachary JF. Differentiation and characterization of rat mammary fibroadenomas and 4T1 mouse carcinomas using quantitative ultrasound imaging. IEEE Trans Med Imaging. 2004 Jun;23(6):764–71.
49. Feleppa E, Kalisz A, Sokil-Melgar J, Lizzi F, Liu T, Rosado A, et al. Typing of prostate tissue by ultrasonic spectrum analysis. IEEE Trans Ultrason Ferroelectr Freq Control. 1996;43(4):609–19.
50. Yang M, Krueger TM, Miller JG, Holland MR. Characterization of Anisotropic Myocardial Backscatter Using Spectral Slope, Intercept and Midband Fit Parameters. Ultrason Imaging. 2007 Apr 1;29(2):122–34.
51. Czarnota GJ, Kolios MC. Ultrasound detection of cell death. Imaging Med. 2010 Feb;2(1):17–28.
52. Sadeghi-Naini A, Papanicolau N, Falou O, Tadayyon H, Lee J, Zubovits J, et al. Low-frequency quantitative ultrasound imaging of cell death in vivo. Med Phys. 2013 Aug;40(8):82901.
53. Gangeh MJ, Sadeghi-Naini A, Diu M, Tadayyon H, Kamel MS, Czarnota G. Categorizing Extent of Tumour Cell Death Response to Cancer Therapy Using Quantitative Ultrasound Spectroscopy and Maximum Mean Discrepancy. IEEE Trans Med Imaging. 2014;33(6):1390–400.
54. Banihashemi B, Vlad R, Debeljevic B, Giles A, Kolios MC, Czarnota GJ. Ultrasound imaging of apoptosis in tumor response: novel preclinical monitoring of photodynamic therapy effects. Cancer Res. 2008 Oct 15;68(20):8590–6.
55. Herbst C, Kosmehl H, Stiller KJ, Berndt A, Eiselt M, Schubert J, et al. Evaluation of microvessel density by computerised image analysis in human renal cell carcinoma. Correlation to pT category, nuclear grade, proliferative activity and occurrence of metastasis. J Cancer Res Clin Oncol. 1998 Jan;124(3–4):141–7.
56. Hochberg Y, Tamhane AC. Multiple Comparison Procedures. Hoboken, NJ, USA: John Wiley & Sons, Inc.; 1987. (Wiley Series in Probability and Statistics).
57. Kutner MH, Nachtsheim C, Neter J, Li W. Applied linear statistical models. McGraw-Hill Irwin; 2005. 1396 p.
58. Garcia-Barros M, Lacorazza D, Petrie H, Haimovitz-Friedman A, Cardon-Cardo C, Nimer S, et al. Host acid sphingomyelinase regulates microvascular function not tumor immunity. Cancer Res. 2004 Nov 15;64(22):8285–91.
59. Carpinteiro A, Dumitru C, Schenck M, Gulbins E. Ceramide-induced cell death in malignant cells. Cancer Lett. 2008 Jun;264(1):1–10.
60. Kolesnick R, Fuks Z. Response to Comments on "Tumor Response to Radiotherapy Regulated by Endothelial Cell Apoptosis". Science. 2003 Dec 12;302(5652):1894e–1894.
61. Chometon G, Jendrossek V. Targeting the tumour stroma to increase efficacy of chemo- and radiotherapy. Clin Transl Oncol. 2009 Feb;11(2):75–81.
62. Paris F, Fuks Z, Kang A, Capodieci P, Juan G, Ehleiter D, et al. Endothelial apoptosis as the primary lesion initiating intestinal radiation damage in mice. Science. American Association for the Advancement of Science; 2001 Jul 13;293(5528):293–7.
63. Park M-T, Oh E-T, Song M-J, Kim W-J, Cho YU, Kim SJ, et al. The radiosensitivity of endothelial cells isolated from human breast cancer and normal tissue in vitro. Microvasc Res. Elsevier Inc.; 2012;84(2):140–8.
64. El Kaffas A, Czarnota GJ. Tumor vascular conundrum: Hypoxia, ceramide, and biomechanical targeting of tumor vasculature. In: Sahgal A, Lo SS, Ma L, Sheehan JP, editors. Image-Guided Hypofractionated Stereotactic Radiosurgery: A Practical Approach to Guide Treatment of Brain and Spine Tumors. 1st ed. Boca Raton: CRC Press; 2016. p. 9.
65. Tran WT, El Kaffas A, Al-Mahrouki A, Gillies C, Czarnota GJ. A review of vascular disrupting agents as a concomitant anti-tumour modality with radiation. J Radiother Pract. 2013 May 2;12(3):255–62.
66. Czarnota GJ. Ultrasound-stimulated microbubble enhancement of radiation response. Biol Chem. 2015 Jan 1;396(6–7):645–57.
67. Schueneman AJ, Himmelfarb E, Geng L, Tan J, Donnelly E, Mendel D, et al. SU11248 maintenance therapy prevents tumor regrowth after fractionated irradiation of murine tumor models. Cancer Res. 2003 Jul;63(14):4009–16.
68. Vasudev NS, Goh V, Juttla JK, Thompson VL, Larkin JMG, Gore M, et al. Changes in tumour vessel density upon treatment with anti-angiogenic agents: relationship with response and resistance to therapy. Br J Cancer. Nature Publishing Group; 2013 Sep 3;109(5):1230–42.
69. Folberg R, Hendrix MJ, Maniotis a J. Vasculogenic mimicry and tumor angiogenesis. Am J Pathol. American Society for Investigative Pathology; 2000 Feb;156(2):361–81.
70. Sadeghi-Naini A, Falou O, Hudson JM, Bailey C, Burns PN, Yaffe MJ, et al. Imaging innovations for cancer therapy response monitoring. Imaging Med. Future Medicine Ltd London, UK; 2012 Jun 25;4(3):311–27.
71. Gangeh MJ, Tadayyon H, Sannachi L, Sadeghi-Naini A, Tran WT, Czarnota G. Computer Aided Theragnosis Using Quantitative Ultrasound Spectroscopy and Maximum Mean Discrepancy in Locally Advanced Breast Cancer. IEEE Trans Med Imaging. 2015;In Press.
72. Sannachi L, Tadayyon H, Sadeghi-Naini A, Tran W, Gandhi S, Wright F, et al. Non-invasive evaluation of breast cancer response to chemotherapy using quantitative ultrasonic backscatter parameters. Med Image Anal. Elsevier B.V.; 2015;20(1):224–36.
73. Brindle K. New approaches for imaging tumour responses to treatment. Nat Rev Cancer. 2008 Feb;8(2):94–107.